


Percolation threshold of curved linear objects

Junmo Lee ¹ and Jaewook Nam ^{1,2,*}

¹*School of Chemical and Biological Engineering, Seoul National University, Seoul 08826, Republic of Korea*

²*Institute of Chemical Process, Seoul National University, Seoul 08826, Republic of Korea*

 (Received 11 September 2020; accepted 24 November 2020; published 22 January 2021)

In this study, we investigate the percolation threshold of curved linear objects, describing them as quadratic Bézier curves. Using Monte Carlo simulations, we calculate the critical number densities of the curves with different curviness. We also obtain the excluded area of the curves. When an excluded area is given, we can find the critical number density of the curves with arbitrary curviness. Apparent conductivity exponents are computed for the curves, and these values are found to be analogous to that of sticks in the percolative region for a junction resistance dominant system. These results can be used to analyze the optoelectrical performance of metal nanowire films because the high-aspect-ratio metal nanowires can be easily curved during coating.

DOI: [10.1103/PhysRevE.103.012126](https://doi.org/10.1103/PhysRevE.103.012126)

I. INTRODUCTION

Transparent conductive films (TCFs) are optically transparent and electrically conductive thin films. Traditionally, indium tin oxide (ITO), which is a doped metal oxide, has been widely used as a TCF in the market for decades [1]. However, brittleness, the impracticability of applying solution-based coating processes, and price fluctuations are the critical drawbacks in the case of ITO. In this regard, two-dimensional networks of high-aspect-ratio conducting nanomaterials such as carbon nanotubes [2,3], graphenes [4,5], and metal nanowires [6,7] have been actively studied [8–10] for use as next-generation TCFs for applications in devices such as flexible touch screens [3,11], flexible solar cells [12,13], and sensors [14]. Networks of metal nanowires, including silver and copper nanowires, are promising candidates being considered to replace ITO [7,15].

TCFs are required to exhibit a certain desired optoelectrical performance in terms of high optical transmittance and low sheet resistance. However, many factors in the case of metal-nanowire networks, such as the length [16], diameter [17], orientation [18,19], and density of nanowires [20,21] and the junction resistance between intersecting nanowires [22–24], influence the optoelectrical performance. In this regard, several studies have been conducted to investigate the effects of these factors and determine which factors are important for achieving the desired optoelectrical performance of the film. According to percolation theory, the electrical conductivity σ of a network of conductive objects exhibits a power-law dependence on the reduced number density $n/n_c - 1$ with a universal conductivity exponent $t \approx 1.3$ in two dimensions as follows:

$$\sigma \propto \left(\frac{n}{n_c} - 1\right)^t, \quad (1)$$

where n denotes the number density, n_c is the critical number density at the percolation threshold, and t is the conductivity exponent [25]. It is necessary to accurately estimate the critical number density of a given system to identify the power-law dependence expressed in Eq. (1). The majority of previous studies have focused on straight linear objects (“sticks”) for analyzing the electrical conductivity and optical transmittance of metal-nanowire networks [20,23,26–28] and considered the previously obtained percolation threshold of sticks [29,30]. Additionally, the percolation threshold of sticks oriented in one direction with certain distributions [18,31] and that of wavy objects [32,33] have also been studied.

According to the previous studies [16,17], a high aspect ratio of metal nanowires is needed to achieve the desired optoelectrical performance that is comparable to that of ITO. For the same number density, the sheet resistance of the network reduces as the aspect ratio of the metal nanowires increases. However, high-aspect-ratio metal nanowires tend to be curved after various coating processes. Figure 1 shows high-resolution images of silver nanowire films fabricated via the bar-coating process of the silver nanowire ink (FlexioInk, Flexio Co., Ltd., Korea). The images were obtained via scanning electron microscopy (SEM, JSM-7800F Prime JEOL Ltd., Japan). The silver nanowires in both images are clearly curved linear objects. Nevertheless, the effect of the curviness on percolation has not been thoroughly investigated thus far. Consequently, we present a simplified model system herein to analyze this effect.

II. METHODS

A. Representation of a curved linear object

The curved linear objects considered in this study are described as quadratic Bézier curves; in such a curve, control point \mathbf{P}_2 lies on the perpendicular bisector of the line segment between \mathbf{P}_1 and \mathbf{P}_3 . We call this type of curve a “symmetric” quadratic Bézier curve. The curve is expressed as a parametric

*Corresponding author: jaewooknam@snu.ac.kr

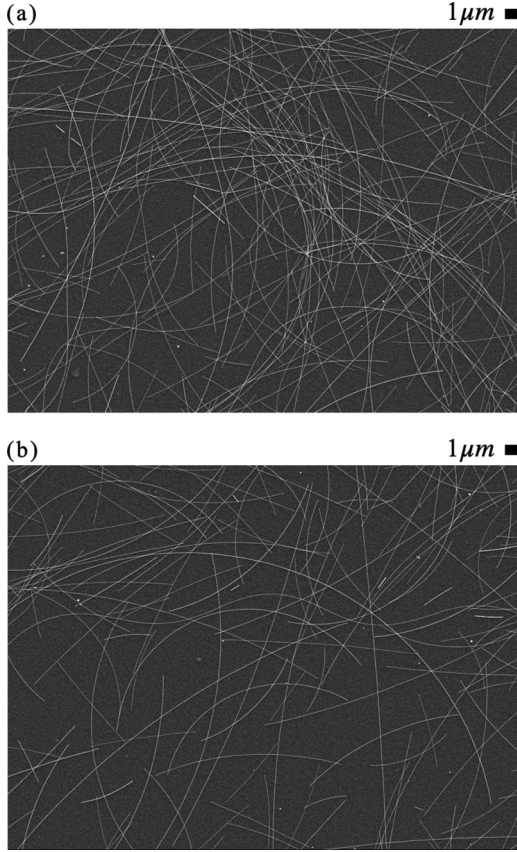


FIG. 1. Scanning electron microscope images of high-aspect-ratio silver nanowire films. The silver nanowires are no longer straight but curved in both (a) the high-number-density network and (b) low-number-density networks.

function given by

$$\begin{aligned} \mathbf{B}(k) &= (B_x, B_y) \\ &= (1-k)^2\mathbf{P}_1 + 2(1-k)k\mathbf{P}_2 + k^2\mathbf{P}_3, \end{aligned} \quad (2)$$

where $k \in [0, 1]$.

Figure 2 shows several parameters of interest for a given curve. The center point \mathbf{c} of the curve is the midpoint of \mathbf{P}_1 and \mathbf{P}_3 . We chose the orientation angle of the curve to be θ ,

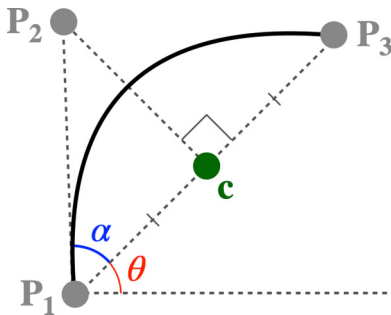


FIG. 2. Symmetric quadratic Bézier curve. The solid black line denotes the curve, and the gray dotted lines represent the horizontal axis and several line segments. \mathbf{P}_1 , \mathbf{P}_2 , and \mathbf{P}_3 represent the control points, \mathbf{c} represents the center point, θ represents the orientation angle, and α represents the curviness angle.

the angle of the line segment between \mathbf{P}_1 and \mathbf{P}_3 with respect to the horizontal axis. The arc length of the curve can be obtained as

$$l = \int_0^1 \sqrt{\left(\frac{dB_x}{dk}\right)^2 + \left(\frac{dB_y}{dk}\right)^2}. \quad (3)$$

To quantify the degree of curviness of the curve, we introduce the curviness angle α , the angle between the line segment with end points \mathbf{P}_1 and \mathbf{P}_2 and the line segment with end points \mathbf{P}_1 and \mathbf{P}_3 . As α increases, the degree of curviness increases. Furthermore, α is bounded in the interval $0^\circ \leq \alpha < 90^\circ$. When $\alpha = 0^\circ$, the curve becomes a perfectly straight line, which is a convex object. However, when $0^\circ < \alpha < 90^\circ$, it turns into a nonconvex object that has been considered by only a few studies. It must be noted that the nonconvex objects can intersect more than twice. Furthermore, the percolation properties of the nonconvex objects are mostly unknown. When $\alpha \rightarrow 90^\circ$, \mathbf{P}_1 approaches \mathbf{P}_3 . In this limit, the curve eventually becomes a half-length stick, which is not considered in this study.

B. Monte Carlo simulation

Monte Carlo simulations were used to generate networks that consist of symmetric quadratic Bézier curves with the parameters specified previously. In each simulation, the curviness angle was fixed, while the orientation angle and the center point followed a uniform distribution. Here, we focus on the effect of the curviness of linear objects on the percolation. We varied the curviness angles from 10° to 80° in steps of 10° . For simplicity, we set $l = 1$. The sizes of the square-shaped simulation domain L in units of l are 4, 8, 16, 32, and 64 to consider the finite-size effect.

An instance of a “just-percolated” system is considered during the simulations for the given parameters. The curves are added one by one until the system percolates, that is, a cluster of the curves extends from one side of the system to the opposite side, as shown in Figs. 3(d)–3(f). Here, we use an efficient algorithm based on Li and Zhang [30] developed for stick percolation, which combines a weighted union-find algorithm with path compression [34,35] and a subcell algorithm [36]. The algorithm for computing percolation probability $R(N, L)$ is summarized in the Appendix.

Considering the available computing power, we performed approximately 10^5 realizations for $L \leq 32$ and approximately 2×10^4 realizations for $L = 64$. The algorithm considered in this study was implemented via an in-house PYTHON code and executed on a computer with an Intel Xeon Gold 6146 CPU at 3.20 GHz with 125 GB RAM. The curves with $\alpha = 30^\circ$, 50° , and 70° are shown in Figs. 3(a)–3(c), and the corresponding percolated systems are shown in Figs. 3(d)–3(f), respectively.

C. Excluded area

The excluded area A_{ex} denotes the minimum area around an object into which the center of another object cannot enter without causing overlapping of the two objects [20,37,38]. The relationship between the excluded area (volume) and the onset of percolation in two (three) dimensions has been widely studied [20,37,39–41]. The average excluded area $\langle A_{\text{ex}} \rangle$ can be obtained by averaging A_{ex} of two objects with all possible

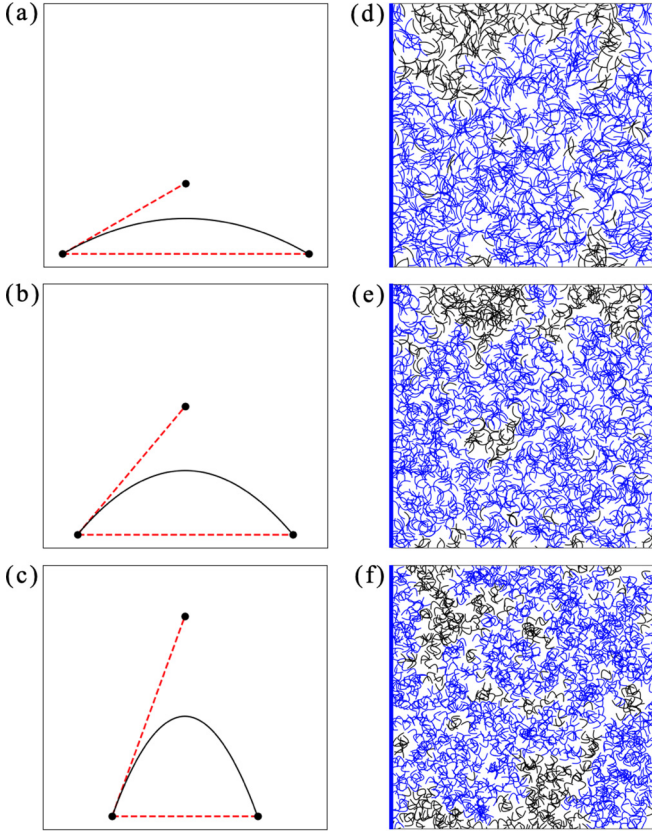


FIG. 3. Symmetric quadratic Bézier curves whose curviness angles are (a) 30°, (b) 50°, and (c) 70° and (d)–(f) their Monte Carlo simulations. In (d)–(f), the system size is 16, and percolating clusters and the boundary sticks are represented in blue.

relative orientations. The critical total average excluded area is defined as

$$\langle A_{\text{ex,tot}} \rangle = n_c \langle A_{\text{ex}} \rangle. \tag{4}$$

The critical total average excluded area is invariant for all-parallel soft-core objects [37]. In the continuum two-dimensional isotropic system, the bound $\langle A_{\text{ex,tot}} \rangle = 3.2\text{--}4.5$ for nonparallel convex objects is conjectured by Balberg [39].

Unfortunately, there is no general theory for the evaluation of excluded areas of nonconvex objects. For example, one cannot find general extensions of Steiner’s kinematic formulas [42] for nonconvex objects. However, this can be circumvented by using Monte Carlo trials for its estimation. For the curviness angles considered in this study, $\langle A_{\text{ex}} \rangle$ of the symmetric quadratic Bézier curves were calculated numerically following Saar and Manga [43]. The arc length is unity for each curve. In this study, the size of the square simulation box was set to 4. For each curviness angle, a curve with random orientation was positioned at the center of the simulation box. Next, another curve with the same curviness angle was introduced into the simulation box. Here, we note that the orientation and location were randomly determined. For each step, the connectivity of the curves was checked. We repeated this step 10^7 times to obtain the number of curves intersecting the central one. Finally, the average excluded area was obtained by dividing the number of curves intersecting

TABLE I. Critical number densities n_c with 95% confidence intervals (CIs), average excluded areas $\langle A_{\text{ex}} \rangle$, critical total average excluded areas $\langle A_{\text{ex,tot}} \rangle$, and *apparent* conductivity exponents $\tilde{\tau}$.

α	n_c (95% CI)	$\langle A_{\text{ex}} \rangle$	$\langle A_{\text{ex,tot}} \rangle$	$\tilde{\tau}$
0°	5.63726 ^a	0.636620 ^b	3.588792	
10°	5.6542 (5.65189, 5.65652)	0.634846	3.589551	1.40
20°	5.7065 (5.70279, 5.71020)	0.629711	3.593444	1.40
30°	5.8042 (5.80168, 5.80668)	0.620788	3.603167	1.41
40°	5.9694 (5.96669, 5.97221)	0.606773	3.622099	1.41
50°	6.2457 (6.24291, 6.24840)	0.586339	3.662072	1.41
60°	6.7358 (6.73426, 6.73736)	0.556683	3.749712	1.41
70°	7.7344 (7.72150, 7.74738)	0.506997	3.921339	1.40
80°	10.3331 (10.32292, 10.34324)	0.401144	4.145053	1.42

^a $n_{\text{c,sticks}}$ from Ref. [30].

^bThe actual value is $2/\pi$ from Ref. [37].

the central one by the number of trials (10^7) and multiplying by the area of the simulation box. We averaged $\langle A_{\text{ex}} \rangle$ over 20 calculations.

III. RESULTS AND DISCUSSION

A. Critical number density and average excluded area

In continuum percolation, the number density n , which is defined as the number of objects per unit area, is an important parameter for a given system. Here, we note that the number of objects N is discrete but n is not necessarily so. However, we cannot obtain any n upon dividing N by L^2 directly; hence, we calculate the percolation probability $R(n, L)$. As per Ref. [30], $R(n, L)$ can be obtained by convolving $R(N, L)$ with the Poisson distribution for any n with arbitrary precision:

$$R(n, L) = \sum_{N=0}^{\infty} \frac{\lambda^N e^{-\lambda}}{N!} R(N, L), \tag{5}$$

where $\lambda = nL^2$. The summation in Eq. (5) proceeds until the magnitude of a successive term is smaller than 10^{-20} .

The critical number density estimate $n_{0.5}(L)$ is defined as the number density satisfying $R(n_{0.5}, L) = R_c = 0.5$. In Fig. 4(a), $n_{0.5}(L)$ for each system size can be obtained by the intersection of the dotted horizontal line $R = 0.5$ and each curve.

To obtain the critical number density n_c , we use finite-size scaling as follows:

$$n_{0.5}(L) - n_c \propto L^{-1-1/\nu}, \tag{6}$$

where $\nu = 4/3$ denotes the correlation-length exponent in a two-dimensional system [30,44]. Hence, the critical number density for the thermodynamic limit ($L \rightarrow \infty$) is extracted using the result of linear regression, as shown in Fig. 4(b). For the curviness angles considered in this study, Eq. (6) is suitable, given that the coefficient of determination R^2 is greater than 0.995. The results are listed in Table I, along with the critical number density of the sticks.

As mentioned before, when $\alpha \rightarrow 90^\circ$, the curve becomes a half-length stick. Now, $\langle A_{\text{ex}} \rangle$ becomes 1/4 of that of $\alpha = 0^\circ$, while $\langle A_{\text{ex,tot}} \rangle$ is the same. Hence, there has to be a

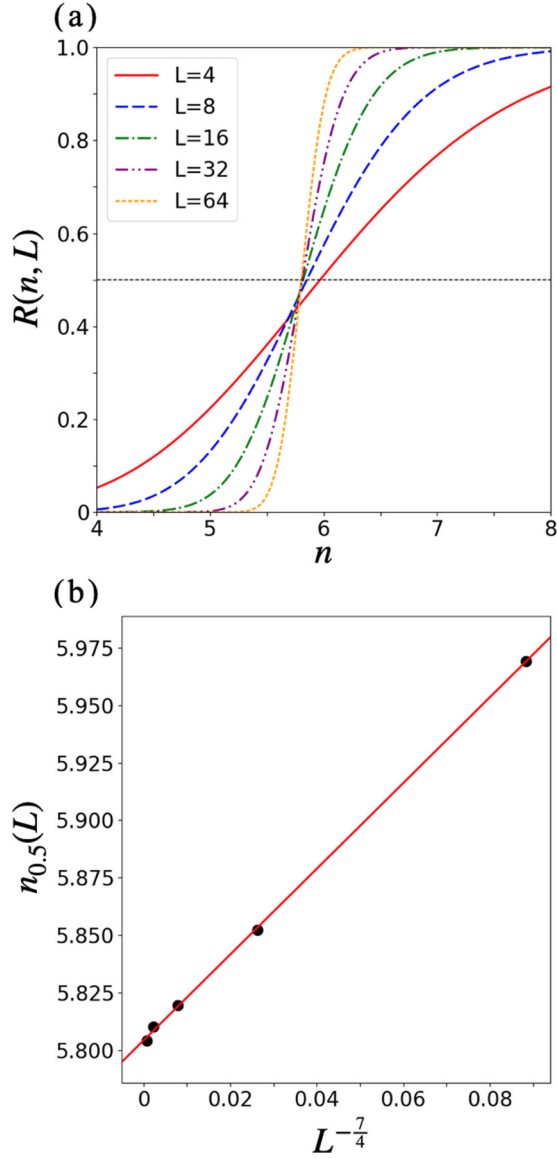


FIG. 4. Monte Carlo simulation results of the curves with curviness angle $\alpha = 30^\circ$ for system sizes $L = 4, 8, 16, 32,$ and 64 . (a) The plot of percolation probability R as a function of the number density n . The horizontal dotted line corresponds to $R = 0.5$. (b) The plot of the critical number density estimate $n_{0.5}$ vs $L^{-1-1/\nu}$ for finite-size scaling. The red line indicates the best fit of the data, which is the result of linear regression with coefficient of determination $R^2 = 0.99969$.

transition from increasing to decreasing $\langle A_{\text{ex,tot}} \rangle$; that is, the maximum of nonconvexity between $\alpha = 70^\circ$ and 90° has to occur.

Over the whole range of curviness angles, $3.5 < \langle A_{\text{ex,tot}} \rangle < 4.2$, as can be observed in Table I. Interestingly, the values of $\langle A_{\text{ex,tot}} \rangle$ of the symmetric quadratic Bézier curves lie in the range of $\langle A_{\text{ex,tot}} \rangle$ reported by Balberg [39]. It must be noted that our curves are nonconvex objects, whereas the range was estimated using nonparallel convex objects in the continuum two-dimensional isotropic system.

Following Li and Östling [40], we next introduce the correction factor $n_{c0} = -2.46$, and the relation

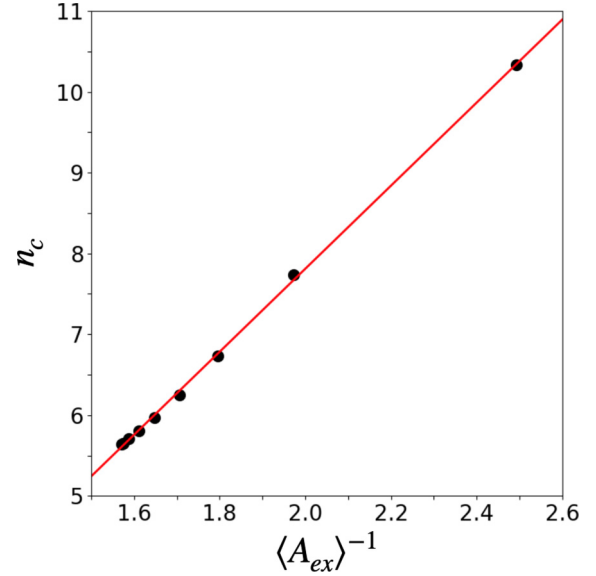


FIG. 5. Critical number density n_c as a function of the reciprocal of the average excluded area $\langle A_{\text{ex}} \rangle^{-1}$. The red line indicates the best fit of the data, which is the result of linear regression with the coefficient of determination $R^2 = 0.99943$. The data point at $\langle A_{\text{ex}} \rangle = 0.636620$ is computed from the stick corresponding to $\alpha = 0^\circ$.

becomes

$$n_c + 2.46 = 5.14l^2 / \langle A_{\text{ex}} \rangle. \quad (7)$$

We can therefore derive the relation between the critical number density of the curves and that of sticks eliminating n_{c0} :

$$n_c = n_{c,\text{sticks}} + 5.14 [l^2 / \langle A_{\text{ex}} \rangle - l^2 / \langle A_{\text{ex,sticks}} \rangle]. \quad (8)$$

As shown in Fig. 5, this linear relation can successfully predict any critical number density at a given $\langle A_{\text{ex}} \rangle$ without time-consuming Monte Carlo simulations.

B. Conductivity exponent

Several studies have reported on the conductivity exponent t for a network of sticks. According to Li and Zhang [45], the *apparent* conductivity exponent \tilde{t} can be extracted with the conductivity data at n above, but not very close to, n_c . Here, we compute \tilde{t} for the network of symmetric quadratic Bézier curves for comparison with that of sticks. For a junction resistance dominant system, the reported \tilde{t} for sticks lie in the range of $\tilde{t} = 1.4\text{--}1.5$ [20,45].

In this study, we computed the conductivity of the network of the curves using the method proposed by Kim and Nam [26]. The network is represented with a matrix by a multinodal representation model. The network forms a graph containing information about the junctions of the curves and their respective separations [23]. Here, the junctions of the intersecting curves have two vertices each, and the junctions or segments of the curve between junctions form the edges. The corresponding matrix system of Kirchhoff's laws is treated via the block matrix approach. Here, we assume that the internal resistances R_i and junction resistances R_j are constant.

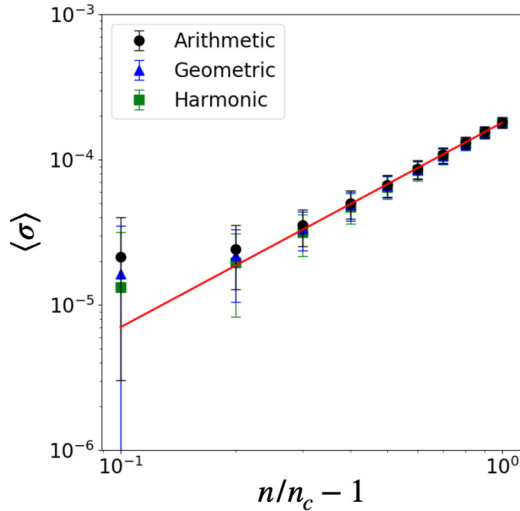


FIG. 6. Three mean conductivities (σ) vs reduced number density for networks of conducting curves with curviness angle $\alpha = 30^\circ$. The ratio of the internal resistance to the junction resistance is set to 10^{-3} , i.e., corresponding to a junction resistance dominant system. The slope of the red line indicates the apparent conductivity exponent ($\tilde{\tau} = 1.41$).

We calculated the conductivities for 1000 networks for each curviness angle with $R_i/R_j = 10^{-3}$ in the percolative region, where $0.1 \leq n/n_c - 1 \leq 1$. Here, we particularly consider a junction resistance dominant system. Following Li and Zhang [45], the arithmetic, geometric, and harmonic means of the conductivities are calculated, as shown in Fig. 6. Subsequently, the conductivity exponent is estimated for the regime $0.3 \leq n/n_c - 1 \leq 1$ via nonlinear regression using the Levenberg-Marquardt algorithm, as the calculated conductivity exponents of the three means are analogous to each other in this regime.

For the curviness angle considered in this study, the apparent conductivity exponents are in the range of $\tilde{\tau} = 1.40$ – 1.42 , as listed in Table I. These values are almost the same as those obtained for the sticks which was reported by Refs. [20,45]. Therefore, we conclude that the power-law dependence does not change owing to the curviness of objects.

IV. CONCLUSIONS

In this study, we considered the percolation of the networks of linear objects, which deviate from that of sticks owing to curviness. Based on this difference, the critical number densities also deviate from those of the sticks. In addition, we determined the relationship between curviness and the critical number density via the excluded area. However, the conductivity exponent of the power-law dependence does not change owing to the curviness of the linear objects.

The critical number densities of linear objects monotonically increase as the curviness angle increases. For practical applications such as the networks of metal nanowires, a higher curviness of nanowires implies that a higher number density is required to achieve the same degree of conductivity. However, the density of nanowires is proportional to the area coverage,

and a larger area coverage reduces the transmittance of the nanowire network [17].

Although a previous study suggested that higher aspect ratios result in higher conductivity, our results imply that the control of the nanowire shape is the key [16]. Typically, high-aspect-ratio nanowires are easily curved during the various coating processes. Therefore, to benefit from a high aspect ratio, a process to ensure that the nanowire is straight must be carefully developed.

Our findings can serve as a basis for future studies: we can optimize the optoelectrical performance of a network of metal nanowires considering not only the aspect ratio but also the curviness of the nanowires. Moreover, if individual nanowires can be extracted automatically from the SEM images of high-aspect-ratio metal nanowire films, we can analyze the factors that need to be considered to improve the performance.

ACKNOWLEDGMENTS

This work was partly supported by the National Research Foundation of Korea (NRF; Grants No. NRF-2018R1A5A1024127 and No. NRF-2020R1A2C2008141) grant funded by the Korean government (MSIT) and the Technology Innovation Program (or Industrial Strategic Technology Development Program; Grant No. 20007256) funded by the Ministry of Trade, Industry and Energy (MOTIE, Korea).

APPENDIX: ALGORITHM FOR MONTE CARLO SIMULATIONS

In our study, the simulation system is split into $L \times L$ square subcells, where the size of the unit subcell is $l \times l$. The center point \mathbf{c} of one curve is generated in position (x, y) using a uniform distribution with random orientation angle θ . We note that $0 \leq x, y \leq L$ and $0 \leq \theta \leq 2\pi$. Each curve is ascribed to the subcell to which the center of the curve belongs. The connectivity needs to be checked only for two sticks belonging to the same and neighboring subcells. For the sake of efficiency of the algorithm, a tree data structure is used to represent the cluster.

Two boundary sticks of length L [e.g., thick blue vertical sticks in Figs. 3(d)–3(f)] form the boundaries of the system facing each other, and each of them is a “root” node in the individual graph tree structure. Subsequently, when a new curve is added with random position and orientation, the connectivity is checked with the two boundary sticks and the curves in the same and neighboring subcells. Three cases exist for connectivity. First, if the curve does not intersect any other curve, it is assigned as the root curve of the new cluster. Second, if the curve intersects existing curves or a boundary stick, the curve belongs to the same cluster, pointing to the root curve or another curve in the cluster. Finally, if the curve belongs to two clusters simultaneously, the clusters are amalgamated as the root curve of one cluster points to the root curve of the other cluster. Pointing to the same root curve directly or indirectly implies that the curves belong to the same cluster.

When two boundary sticks are in the same cluster for the first time, that is, when the system percolates, the number

of sticks is stored as N_f . Finally, the percolation probability $R(N, L)$ for N curves with system size L can be obtained by

dividing the number of N_f satisfying $N_f \leq N$ by the number of realizations.

-
- [1] A. Stadler, *Materials* **5**, 661 (2012).
- [2] J. T. Han, S. Y. Kim, J. S. Woo, and G.-W. Lee, *Adv. Mater.* **20**, 3724 (2008).
- [3] E. Artukovic, M. Kaempgen, D. Hecht, S. Roth, and G. Grüner, *Nano Lett.* **5**, 757 (2005).
- [4] F. Bonaccorso, Z. Sun, T. Hasan, and A. Ferrari, *Nat. Photonics* **4**, 611 (2010).
- [5] S. Pei, J. Zhao, J. Du, W. Ren, and H.-M. Cheng, *Carbon* **48**, 4466 (2010).
- [6] C.-H. Liu and X. Yu, *Nanoscale Res. Lett.* **6**, 75 (2011).
- [7] S. Ye, A. R. Rathmell, Z. Chen, I. E. Stewart, and B. J. Wiley, *Adv. Mater.* **26**, 6670 (2014).
- [8] S. De and J. N. Coleman, *MRS Bull.* **36**, 774 (2011).
- [9] D. S. Hecht, L. Hu, and G. Irvin, *Adv. Mater.* **23**, 1482 (2011).
- [10] L. Hu, H. Wu, and Y. Cui, *MRS Bull.* **36**, 760 (2011).
- [11] J. Lee, P. Lee, H. Lee, D. Lee, S. S. Lee, and S. H. Ko, *Nanoscale* **4**, 6408 (2012).
- [12] Z. Yang, T. Chen, R. He, G. Guan, H. Li, L. Qiu, and H. Peng, *Adv. Mater.* **23**, 5436 (2011).
- [13] X. Wang, Z. Li, W. Xu, S. A. Kulkarni, S. K. Batabyal, S. Zhang, A. Cao, and L. H. Wong, *Nano Energy* **11**, 728 (2015).
- [14] A. Star, E. Tu, J. Niemann, J.-C. P. Gabriel, C. S. Joiner, and C. Valcke, *Proc. Natl. Acad. Sci. USA* **103**, 921 (2006).
- [15] D. Langley, G. Giusti, C. Mayousse, C. Celle, D. Bellet, and J.-P. Simonato, *Nanotechnology* **24**, 452001 (2013).
- [16] R. M. Mutiso, M. C. Sherrott, A. R. Rathmell, B. J. Wiley, and K. I. Winey, *ACS Nano* **7**, 7654 (2013).
- [17] S. M. Bergin, Y.-H. Chen, A. R. Rathmell, P. Charbonneau, Z.-Y. Li, and B. J. Wiley, *Nanoscale* **4**, 1996 (2012).
- [18] J. Mietta, R. M. Negri, and P. I. Tamborenea, *J. Phys. Chem. C* **118**, 20594 (2014).
- [19] M. Jagota and N. Tansu, *Sci. Rep.* **5**, 10219 (2015).
- [20] R. M. Mutiso and K. I. Winey, *Phys. Rev. E* **88**, 032134 (2013).
- [21] H. G. Manning, C. G. da Rocha, C. O'Callaghan, M. S. Ferreira, and J. J. Boland, *Sci. Rep.* **9**, 1 (2019).
- [22] A. T. Bellew, H. G. Manning, C. Gomes da Rocha, M. S. Ferreira, and J. J. Boland, *ACS Nano* **9**, 11422 (2015).
- [23] C. G. da Rocha, H. G. Manning, C. O'Callaghan, C. Ritter, A. T. Bellew, J. J. Boland, and M. S. Ferreira, *Nanoscale* **7**, 13011 (2015).
- [24] F. Selzer, C. Floresca, D. Knepe, L. Bormann, C. Sachse, N. Weiß, A. Eychmüller, A. Amassian, L. Müller-Meskamp, and K. Leo, *Appl. Phys. Lett.* **108**, 163302 (2016).
- [25] D. Stauffer and A. Aharony, *Introduction to Percolation Theory* (CRC Press, Boca Raton, FL, 2018).
- [26] D. Kim and J. Nam, *J. Appl. Phys.* **124**, 215104 (2018).
- [27] F. Han, T. Maloth, G. Lubineau, R. Yaldiz, and A. Tevtia, *Sci. Rep.* **8**, 1 (2018).
- [28] D. Kim and J. Nam, *J. Phys. Chem. C* **124**, 986 (2019).
- [29] G. Pike and C. Seager, *Phys. Rev. B* **10**, 1421 (1974).
- [30] J. Li and S.-L. Zhang, *Phys. Rev. E* **80**, 040104(R) (2009).
- [31] Y. Y. Tarasevich and A. V. Eserkepov, *Phys. Rev. E* **98**, 062142 (2018).
- [32] L. Berhan and A. M. Sastry, *Phys. Rev. E* **75**, 041121 (2007).
- [33] C. Li, E. T. Thostenson, and T.-W. Chou, *Compos. Sci. Technol.* **68**, 1445 (2008).
- [34] M. E. J. Newman and R. M. Ziff, *Phys. Rev. Lett.* **85**, 4104 (2000).
- [35] M. E. J. Newman and R. M. Ziff, *Phys. Rev. E* **64**, 016706 (2001).
- [36] T. Vicsek and J. Kertesz, *J. Phys. A* **14**, L31 (1981).
- [37] I. Balberg, C. H. Anderson, S. Alexander, and N. Wagner, *Phys. Rev. B* **30**, 3933 (1984).
- [38] L. Onsager, *Ann. N.Y. Acad. Sci.* **51**, 627 (1949).
- [39] I. Balberg, *Phys. Rev. B* **31**, 4053 (1985).
- [40] J. Li and M. Östling, *Phys. Rev. E* **88**, 012101 (2013).
- [41] J.-F. Thovert, V. V. Mourzenko, and P. M. Adler, *Phys. Rev. E* **95**, 042112 (2017).
- [42] R. Rosso, *Mol. Phys.* **106**, 2487 (2008).
- [43] M. O. Saar and M. Manga, *Phys. Rev. E* **65**, 056131 (2002).
- [44] R. M. Ziff and M. E. J. Newman, *Phys. Rev. E* **66**, 016129 (2002).
- [45] J. Li and S.-L. Zhang, *Phys. Rev. E* **81**, 021120 (2010).